Sample Analysis Report

June 2011

Customer Undisclosed

Sample Information

Samples A and B were dispersed in 1% SDBS/D_2O as follows:
A portion of the sample was dispersed by 1 hour of tip ultrasonication (cooled; 50% duty cycle at less than 10 W power). It was then centrifuged for 20 minutes at ca. 13,000 x g and the supernatant was collected.

Measurements Performed (NS2 NanoSpectralyzer)

NIR emission spectra using four excitation wavelengths

Absorption spectra from 400 to 1600 nm

Raman spectra using 671 nm laser excitation

Measurement Results and Interpretation

As received, the samples contained visible fine particles suggesting partial aggregation or incomplete dispersion. NIR emission from Sample A was much weaker than from an optimum SWCNT dispersion, so it was also measured after 20 minutes of tip sonication. This sonication increased NIR emission by approximately a factor of 4.

Fluorescence spectra were acquired with total integration times of 10 to 80 s per spectrum. Each Raman spectrum was acquired in 100 s.

Sample A

Figures 1 - 4 show measured NIR emission spectra of the aqueous dispersed samples, along with simulations from the global fitting process. The NIR emission levels were quite low, suggesting that the sample had undergone some chemical sidewall damage or accidental derivatization, or was persistently aggregated. Emission line widths were larger than normal for a well dispersed SWCNT sample. Global fitting was unable to provide spectral simulations with the accuracy seen with better samples. This may reflect energy transfer from small diameter to larger diameter SWCNTs within aggregates.

The absorption spectrum in Fig. 5 shows relatively broad resonant features and a strong diffuse background, both of which are consistent with a perturbed sample.

Figure 6 shows the Raman spectrum, which appears rather normal for a SWCNT sample. Several RBM bands are visible, in addition to a strong G band near 1585 cm^{-1} with a characteristic semiconducting shape, a relatively small D band near 1300 cm^{-1} arising from SWCNT defects, and a D' or 2D band near 2600 cm^{-1}.

The deduced (*n*,*m*) distribution is displayed in Fig. 7 as a graphene sheet plot, with border thickness proportional to species concentration. These results have been corrected by the best current values for structure-dependent fluorimetric brightness. The most abundant species appear to be n-m=1 and n-m=2 structures such as (6,5), (7,5),..(8,7), although a number of others are also present. The oddities in this sample's spectra (from aggregation, energy transfer, or damage) make many of these specific abundance

values uncertain. Figure 8 converts the distribution into a diameter histogram. The average diameter is deduced to be 0.96 nm, with a standard deviation of 0.38 nm. Note that this deduced distribution is significantly wider than distributions deduced for other samples containing similar material with fewer spectral anomalies.

Sample B

Figures 9-12 show measured NIR emission spectra of the aqueous dispersed samples. The main SWCNT band visible is the feature near 6400 cm^{-1}, which may come from (16,2), (10,9), or other SWCNTs with diameters in the 1.30 to 1.36 nm range. There is also a weaker band near 6690 cm^{-1}. (Note: the sharp feature at 10,200 cm^{-1} in Fig. 12 is actually Raman scattering from the SWCNT G' mode, not fluorescence. The fact that Raman scattering is comparable in strength to fluorescence indicates that fluorescence emission is very weak from this sample.) Emission from other species in the sample probably lies at longer wavelengths beyond the limit of the standard InGaAs detector. (However, the instrument can be configured with an extended range detector as an option.) No detailed (*n*,*m*) analysis is possible because so few emission features were captured here.

Figure 13 shows the absorption spectrum. As expected for a sample with large average diameter, essentially no (*n*,*m*)-level spectral detail is visible here. The broad band near 1000 nm may be assigned to the E_{22} transitions of semiconducting SWCNTs in the sample, and the features near 700 nm may be from the first optical transitions of the metallic SWCNTs.

Figure 14 shows the Raman spectrum for Sample B. It is much weaker than that of Sample A. There is an RBM band near 168 cm^{-1}, a G' (2D) band near 2610 cm^{-1}, and an unusually shaped G band. The G band actually has two components. There is a sharp peak near 1582 cm^{-1} (assigned to semiconducting SWCNTs) which is almost obscured by a much wider feature peaking at 1557 cm^{-1}, assigned to a metallic SWCNT species in resonance with the excitation laser. The negative peak near 2350 cm^{-1} corresponds to the O-D stretch of the solvent and occurs because of a minor mismatch in D_2O concentration between sample and reference.

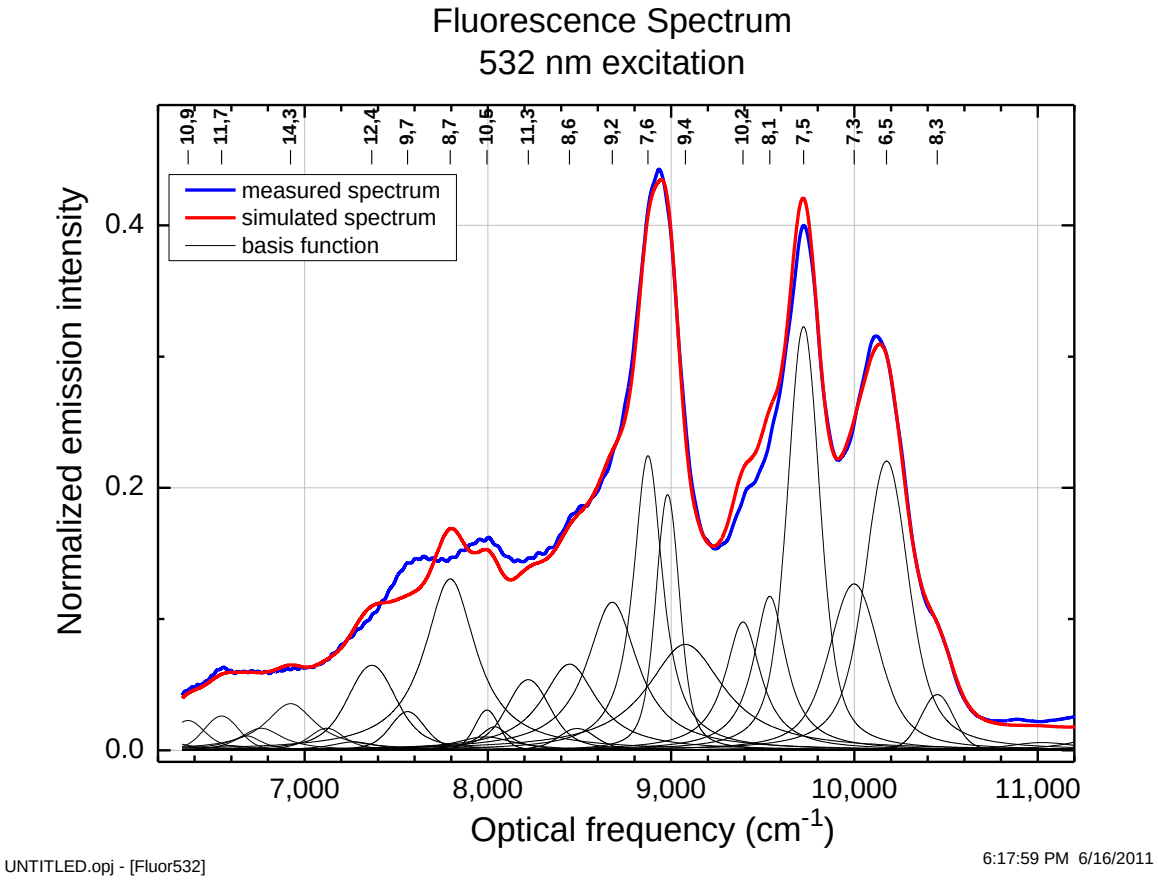

Fig. 1. NIR fluorescence spectrum (and fit) of Sample A, with 532 nm excitation.

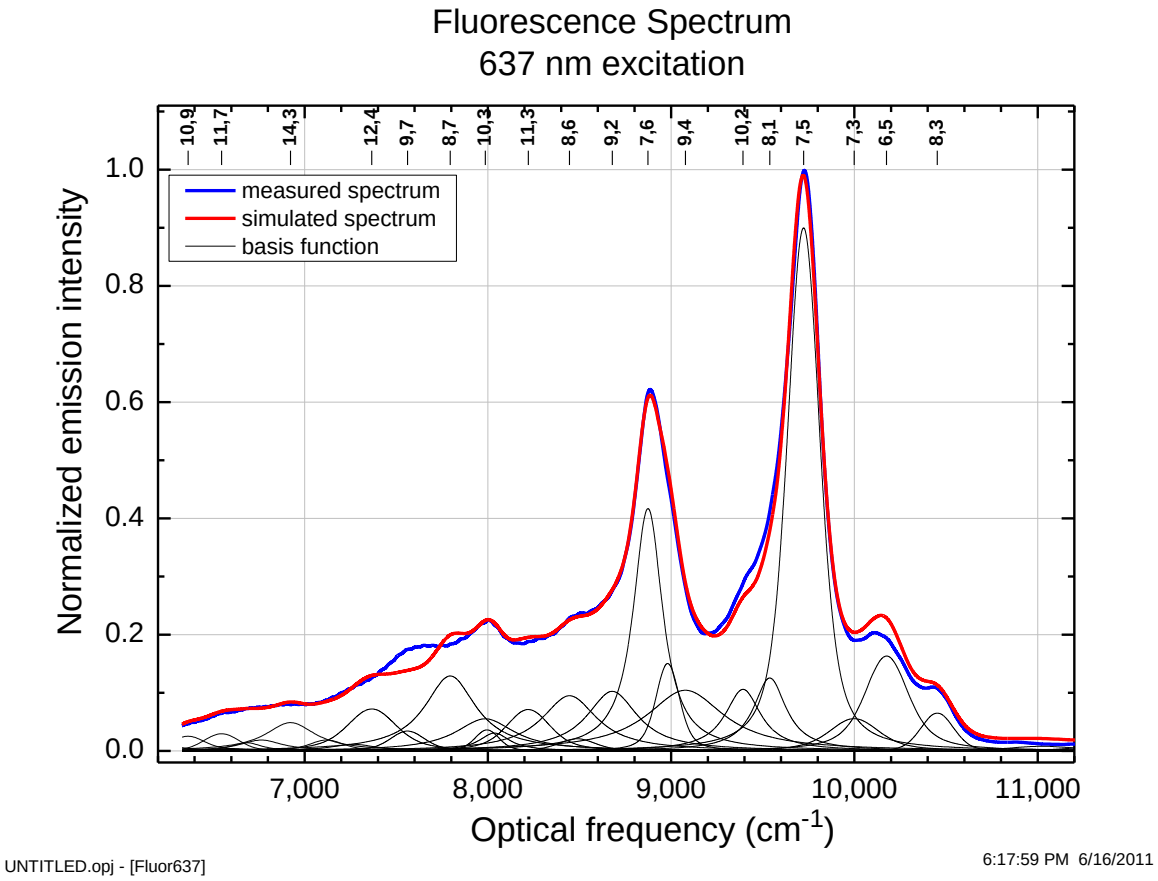

Fig. 2. NIR fluorescence spectrum (and fit) of Sample A, with 637 nm excitation.

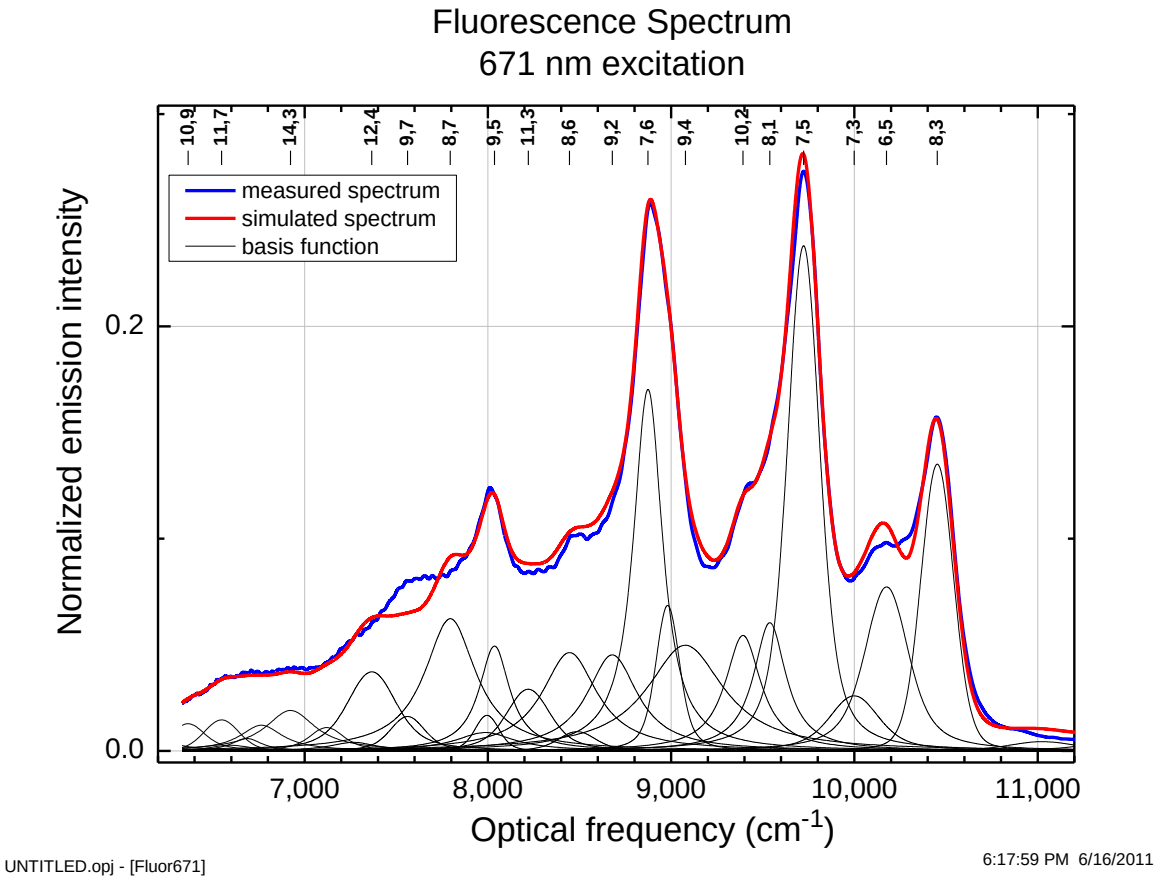

Fig. 3. NIR fluorescence spectrum (and fit) of Sample A, with 671 nm excitation.

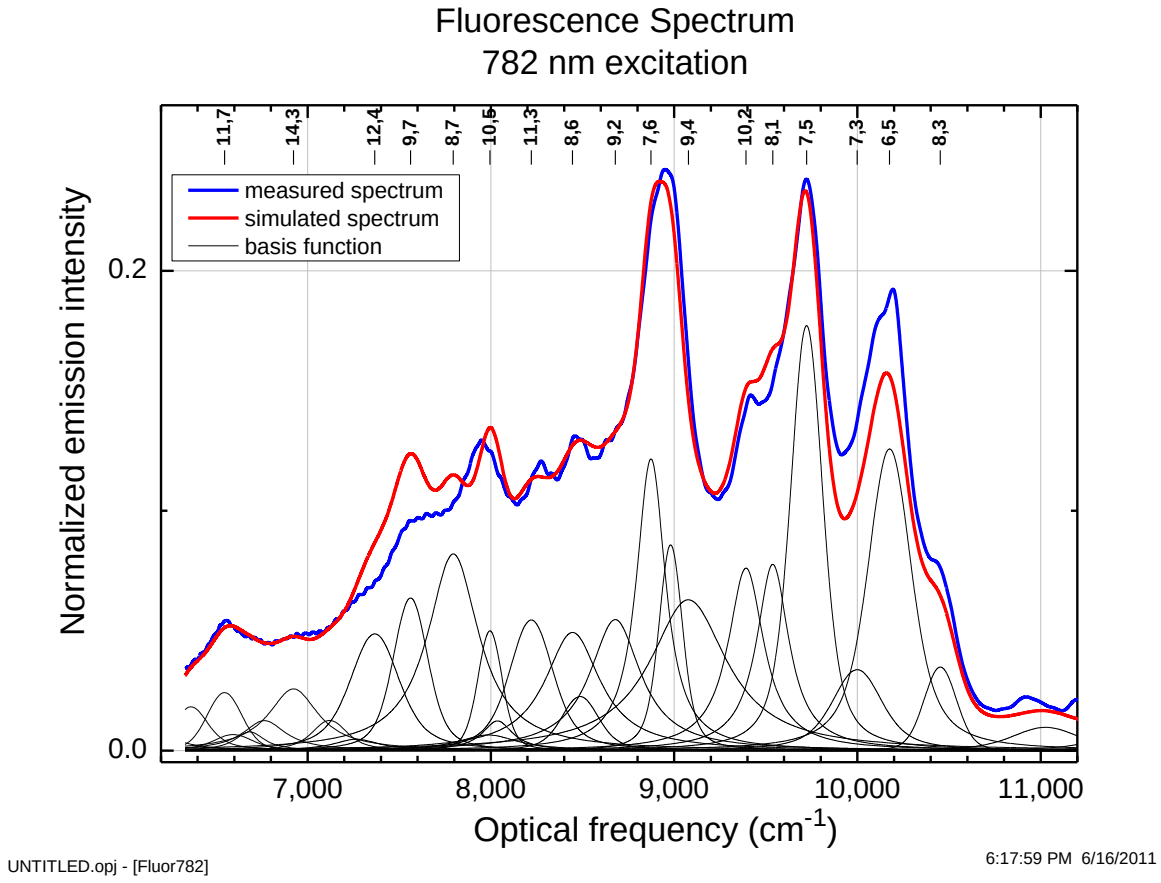

Fig. 4. NIR fluorescence spectrum (and fit) of Sample A, with 782 nm excitation.

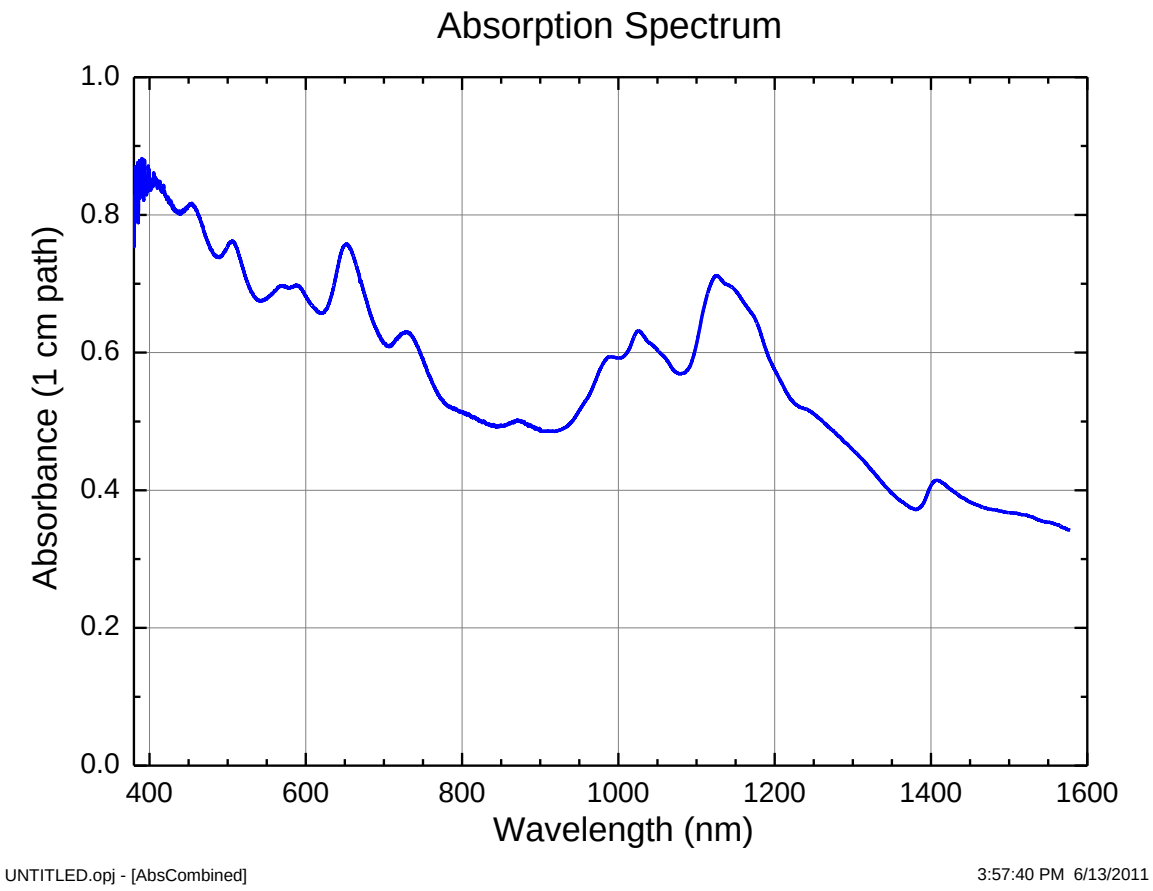

Fig. 5. Vis-NIR absorption spectrum of Sample A.

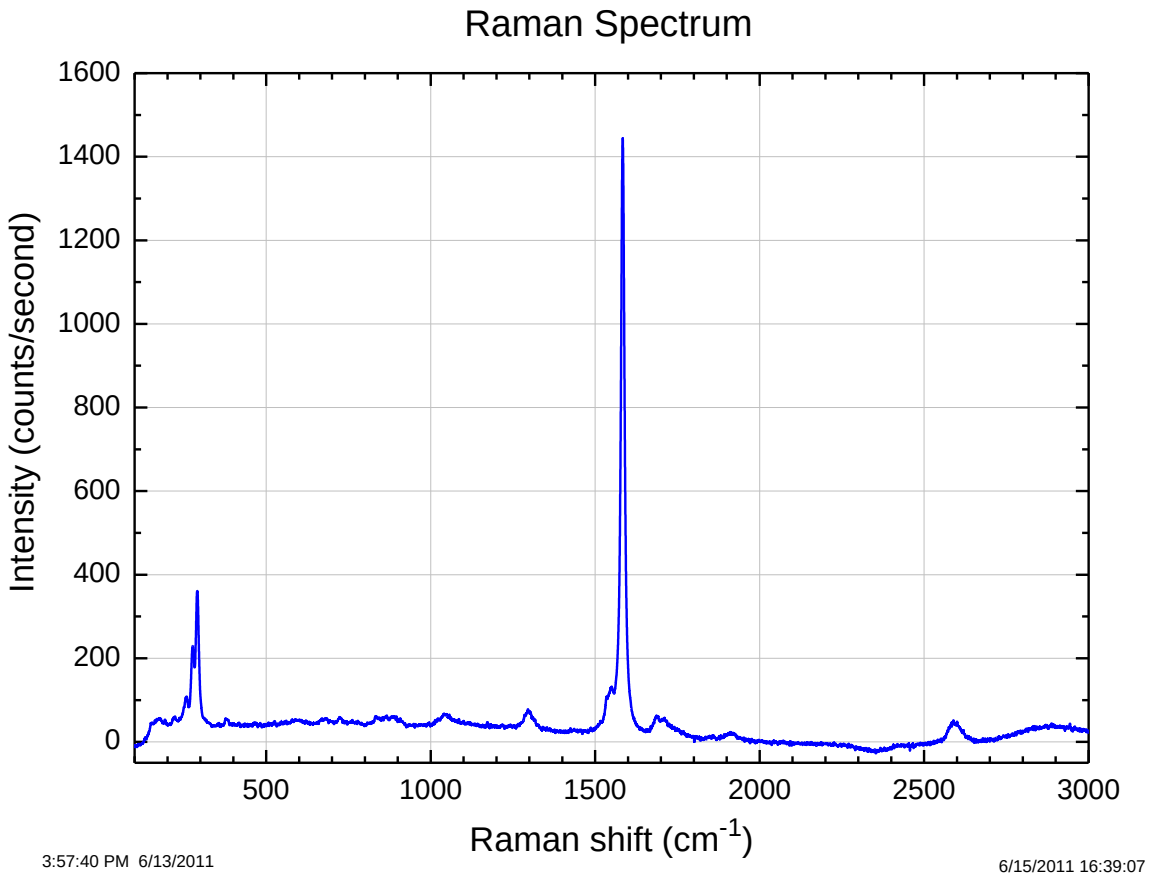

Fig. 6. Raman spectrum of Sample A, with 671 nm excitation.

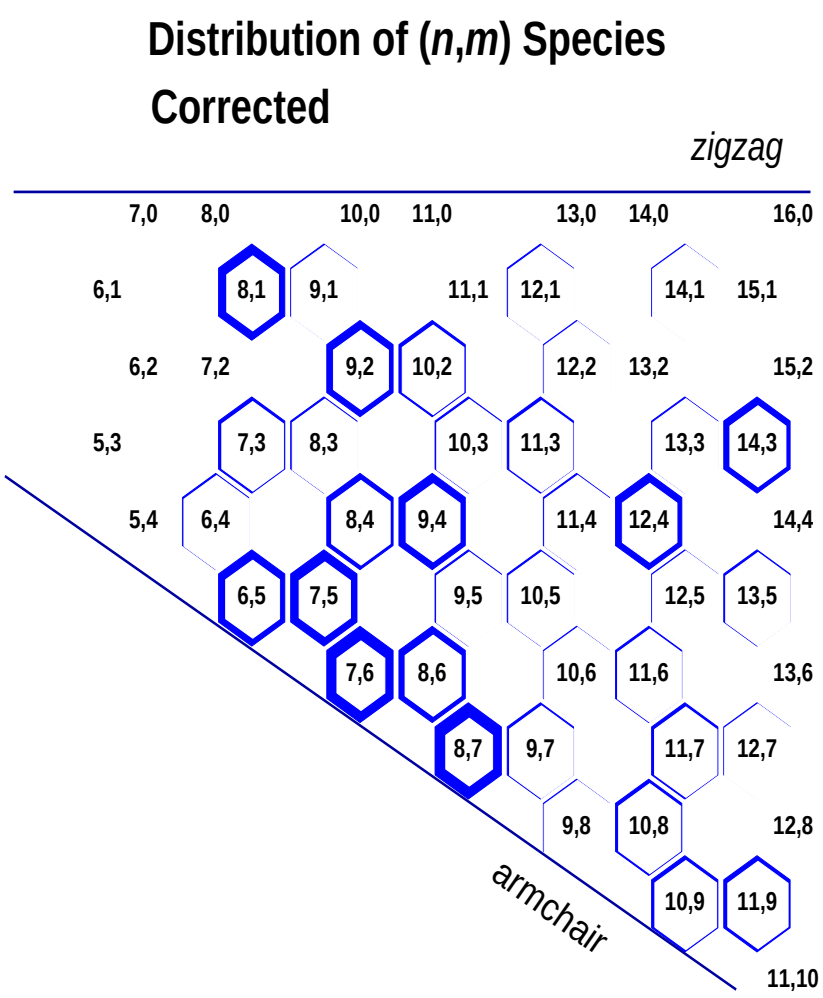

Fig. 7. Graphene sheet plot showing deduced (n,m) distribution of Sample A**.**

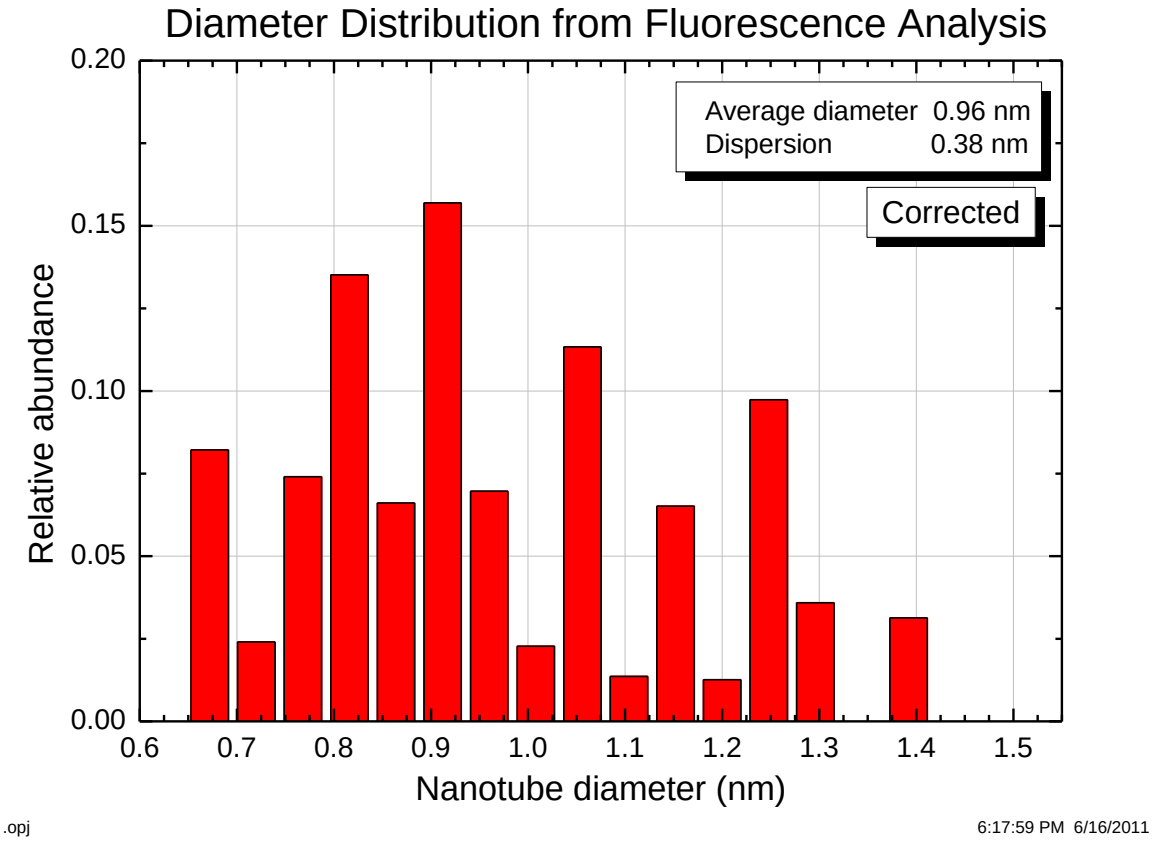

Fig. 8. Histogram plot showing deduced diameter distribution of Sample A**.**

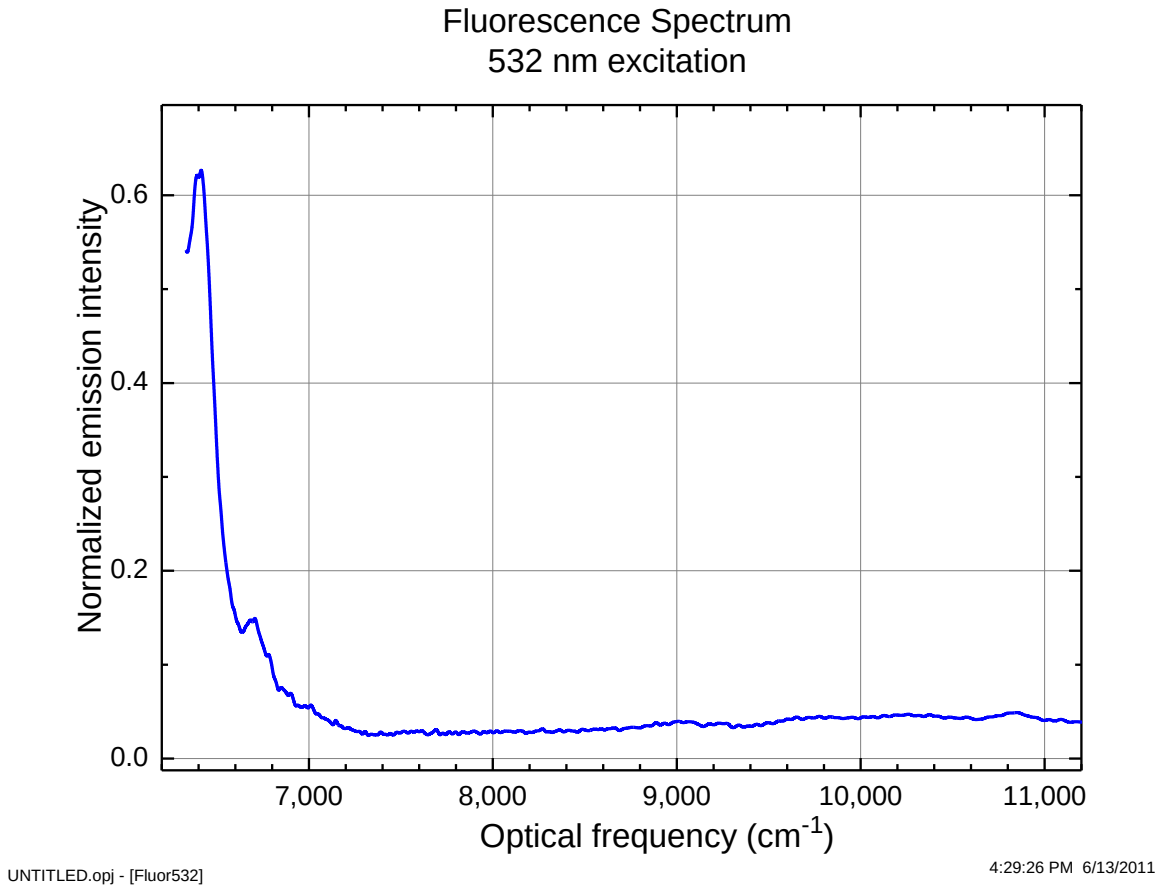

Fig. 9. NIR fluorescence spectrum of Sample B, with 532 nm excitation.

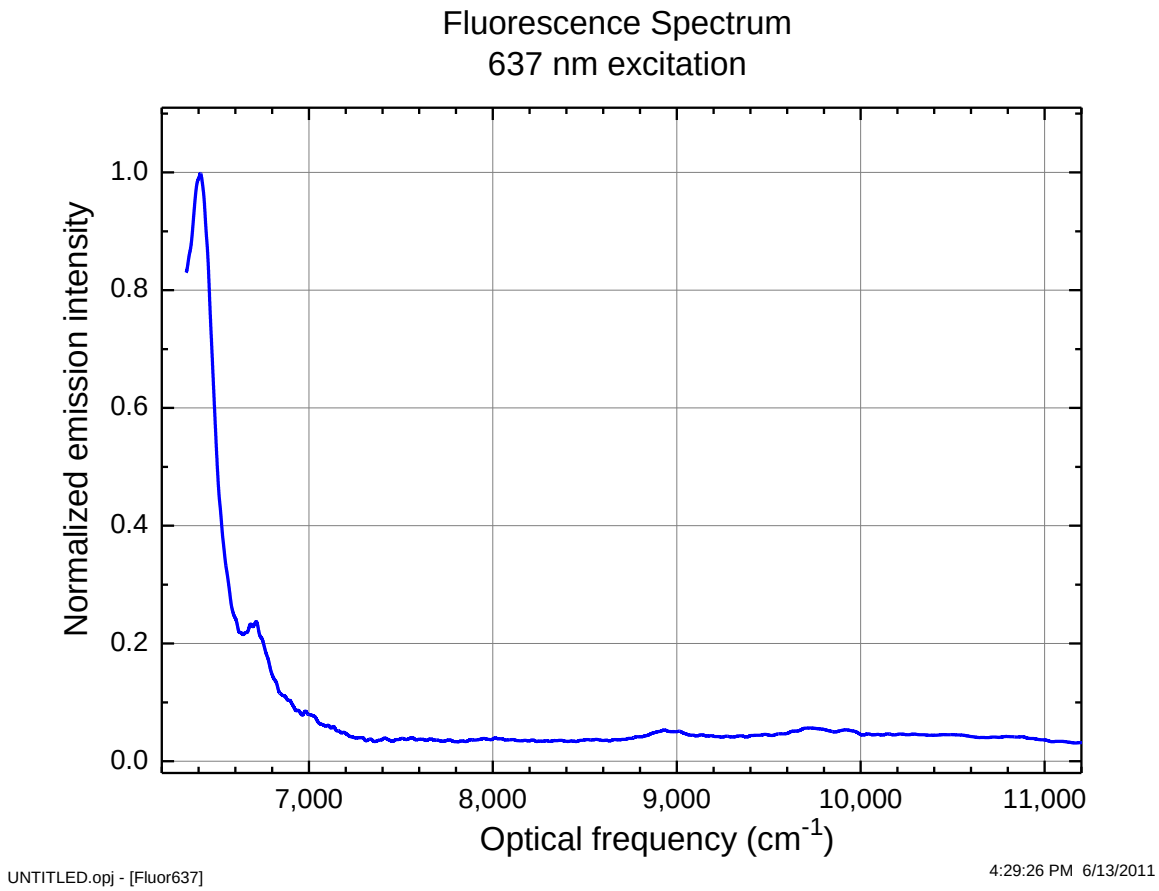

Fig. 10. NIR fluorescence spectrum of Sample B, with 637 nm excitation.

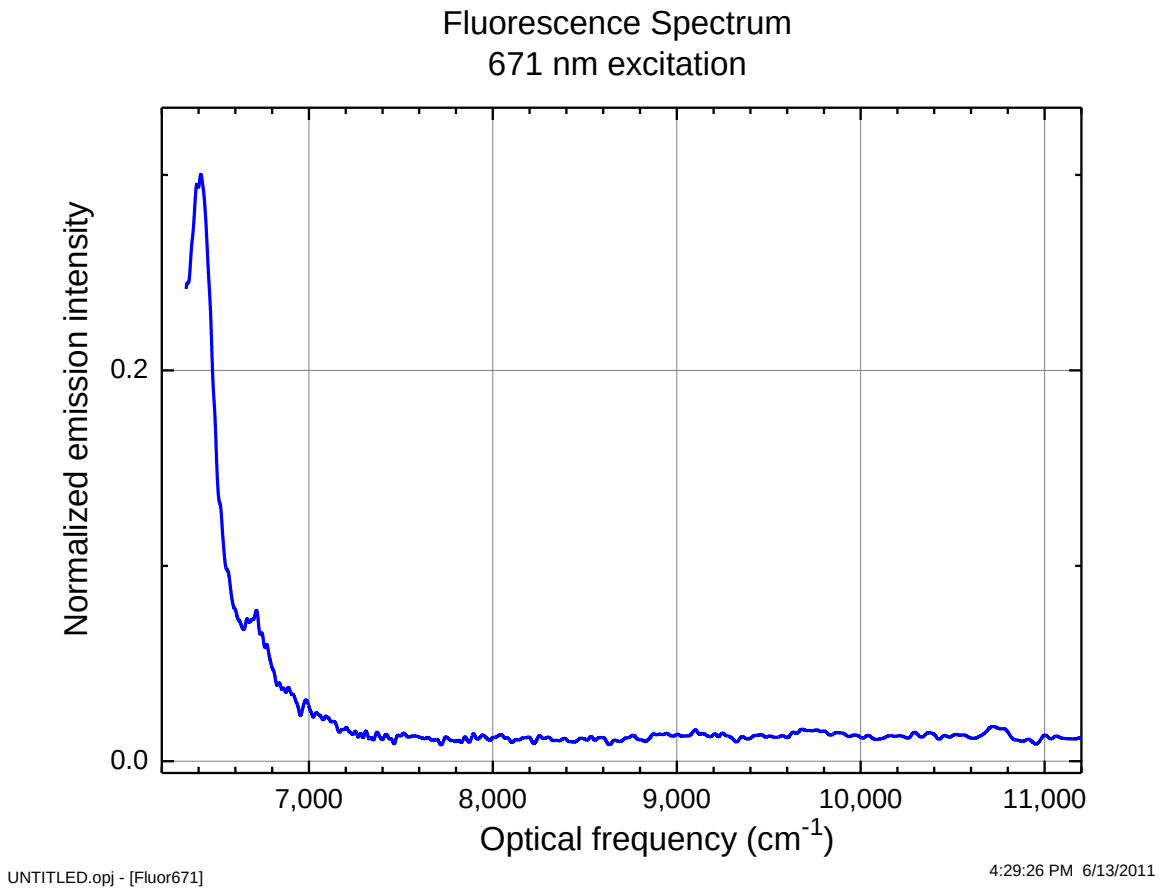

Fig. 11. NIR fluorescence spectrum of Sample B, with 671 nm excitation.

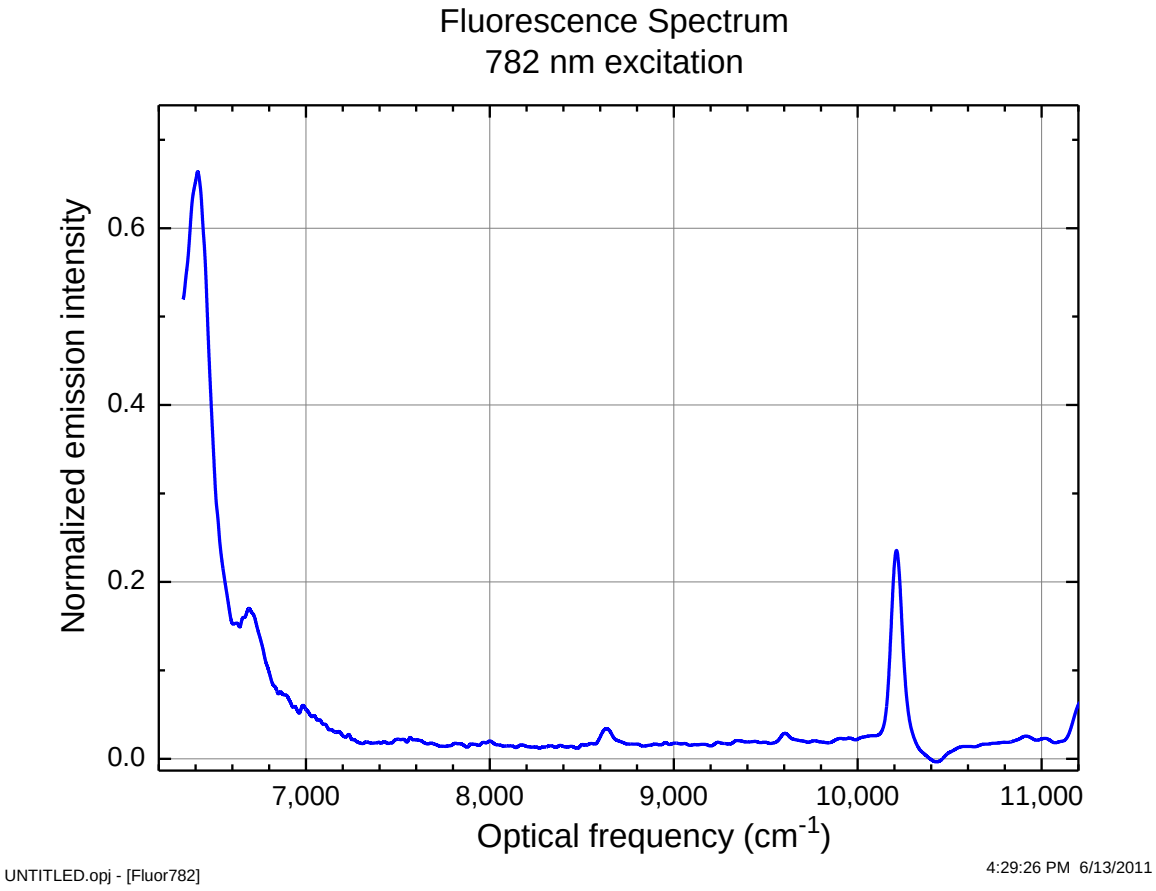

Fig. 12. NIR fluorescence spectrum of Sample B, with 782 nm excitation.

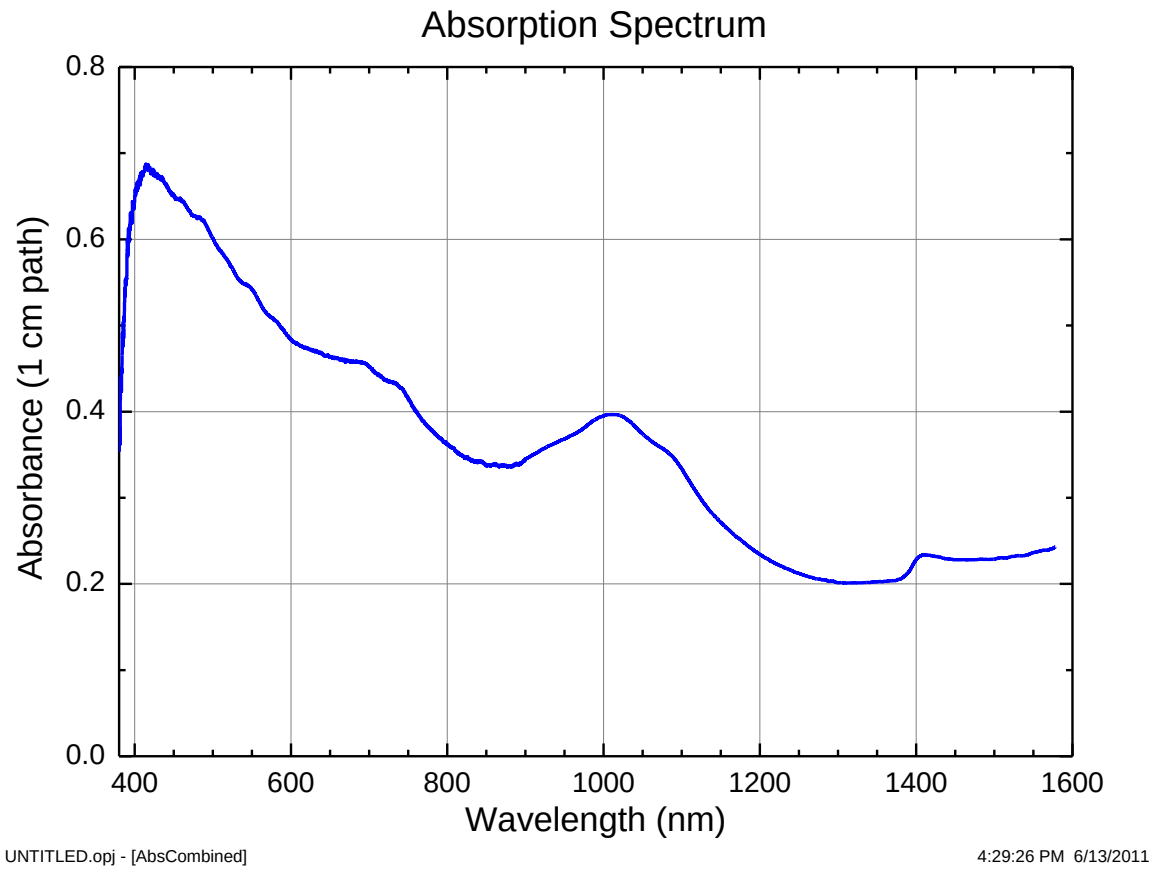

Fig. 13. Vis-NIR absorption spectrum of Sample B.

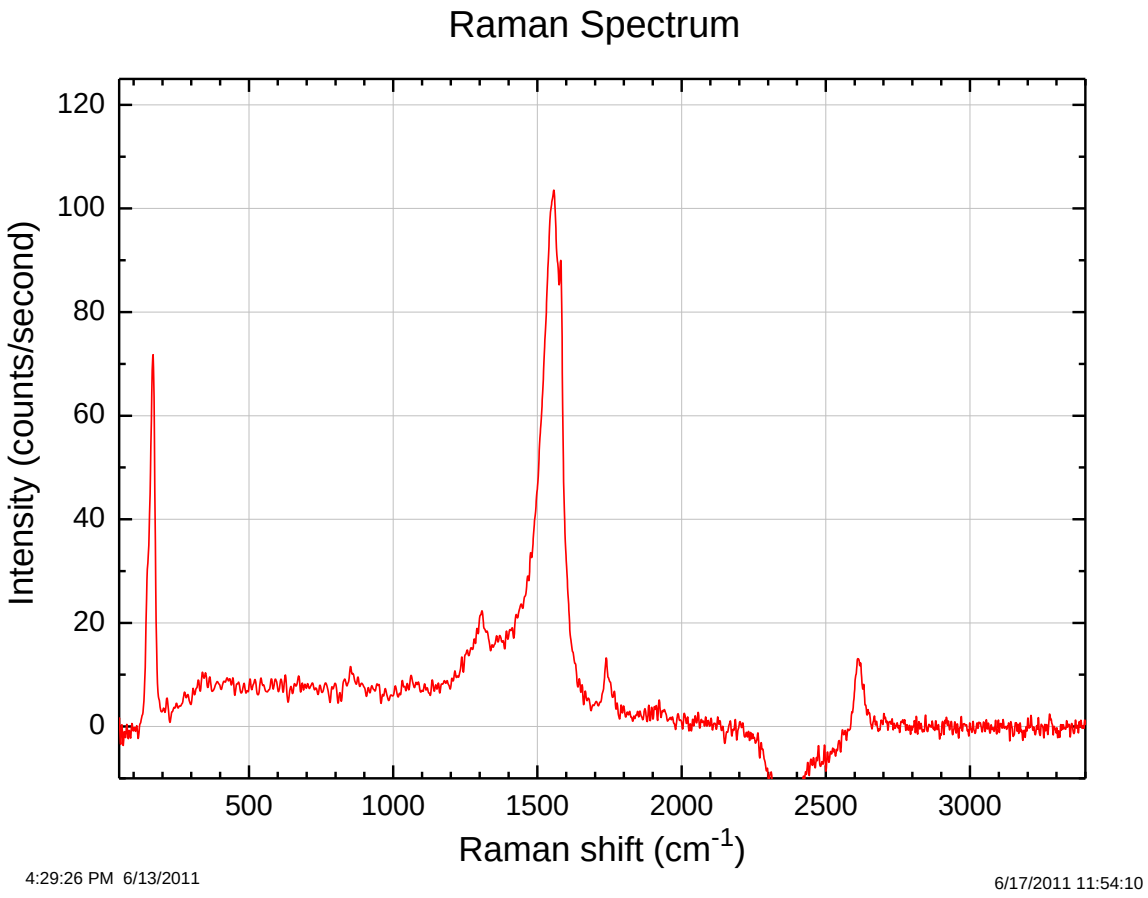

Fig. 14. Raman spectrum of Sample B, with 671 nm excitation.